AWTEC 2012
Asian Wave and Tidal Conference Series
Nov. 27-30, Jeju Island, Korea

1st awtec 2012
Asian Wave and Tidal Energy Conference Series

Performance Studies on a Direct Drive Turbine for Wave Power Generation in a Numerical Wave Tank

Deepak Prasad[1], Mohammed Rafiuddin Ahmed[1,#] and Young – Ho Lee[2]

1 Discipline of Mechanical Engineering, The University of the South Pacific, Suva, Fiji Islands
2 Division of Mechanical & Energy System Engineering, College of Engineering, Korea Maritime University, Busan, South Korea
Corresponding Author / E-mail: ahmed_r@usp.ac.fj, TEL: +679 32 32042, FAX: +679 32 31538

KEYWORDS : Numerical wave tank, CFD, flow characteristics, direct drive turbine

Studying wave characteristics and performance of wave energy convertors is very important. This can be achieved by conducting model tests in physical wave tanks. However, model testing requires significant money and time investment. At times the size of the prototype is big and requires large open space for construction and testing. In addition to this, it is difficult to conduct tests at all operating conditions and design variables with respect to time line and budget. A logical and simple solution is to utilize numerical methods such as the use of Computational Fluid Dynamics (CFD) software. In the current study, a commercial code ANASYS-CFX is used to simulate a numerical wave tank (NWT). The waves in the NWT are generated using a piston type wave-maker which was located at the inlet of the wave tank. The maximum turbine power is obtained at 35 rpm both experimentally and numerically. The results of CFD simulation show good agreement with the experimental data with the difference less than 3%. From CFD analysis, the maximum power is 6.71 W compared to 6.8 W obtained experimentally. The efficiency at 35 rpm is 44.73% and 45.33% respectively from CFD and experiments.

NOMENCLATURE

A = Amplitude
A_{CS} = cross sectional area
c = phase velocity
C_f = first stage energy conversion factor
c_g = group velocity
d = water depth
E = energy density
g = acceleration due to gravity
H = wave height
ΔH = head difference
L_o = length of the front guide nozzle
P_{Avail} = available power at front guide nozzle inlet
P_T = turbine power
P_{Wave} = wave energy flux
P_{WP} = water power
Q = volume flow rate
t = timestep
T = wave period
T_{ave} = average turbine torque
V = volume
W_G = front guide nozzle inlet width
x = horizontal distance
x_{dis} = wave-maker displacement
$\triangle Y$ = rear chamber water level difference
η_T = turbine efficiency
λ = wavelength
ρ = water density
ω = angular velocity
ω_0 = frequency

1. Introduction

A wave tank is characterized as a long and narrow enclosure with a wave-maker at one end [1]. Wave tanks or sometimes referred to as wave flumes have been regularly used in naval engineering, coastal engineering, hydrodynamic studies, studying offshore structures and many other important engineering applications. Waves in the wave tank are generated through the movement of a paddle (also known as a wave-maker) that is located at one of the ends of the wave flume [2].

The most common of these wave-makers are piston, flap and wedge type. The difference amongst these wave-makers solely lies in their motion. A flap type wave-maker is good for generating deep water waves while a piston type wave-maker can be employed to generate shallow or at times intermediate waves [3]. The waves are generated by the oscillating motion of the paddle. The size of the waves generated depends on the wave period, the water depth in front of the wave-maker and the rate of actuation of the paddle. Upon achieving desired wave conditions, tests are then conducted.

Wave tanks have been used over the years to provide helpful information on wave characteristics and employed to conduct prototype testing, however, this can be an expensive and time consuming exercise. On many occasions, time is a major constraint which prevents conducting tests at all operating conditions and design variables. To overcome these issues nowadays much effort is focused on the development of numerical wave tank (NWT). Using numerical methods saves a lot of time and money. It allows for rapid design changes and improvements in very little time. Rapid development in computer technology has paved way to the use of CFD packages in modeling and simulating waves numerically. It is now possible to generate waves of desired characteristics using NWT. With improving computer capabilities it is possible for these CFD packages to solve and give accurate solutions of real life problems.

Researchers have proposed many different varieties of NWT based on specific application. Generally, they can be divided into two groups, one which is based on Non Linear Shallow Water (NLSW) equations and the other based on Navier-Stokes (NS) equations [2]. NWT based on NS equations is generally controlled by either Volume of Fluid (VOF) technique or Smooth Particle Hydrodynamics (SPH) technique. Liu [4], Horko [5] and Repalle [6] have reported the use of VOF method for NWT applications. Papers by Lemos [7] and Van Gent et al. [8] also highlighted the use of this model. On the other hand, Dalrymple and Rodgers [9] employed the SPH model in their simulations to study plunging type wave breaking. This model was also used by Shao et al. [10] to investigate overtopping in coastal structures.

Koo and Kim [11] studied nonlinear waves and forces induced by a wedge type wave-maker in potential theory-based fully nonlinear 2D NWT. In a paper by Finnegan and Goggins [12], 2D NWT was used to simulate linear deep water waves and linear waves for finite depth. Li and Lin [13] studied nonlinear wave-body interaction for a stationary floating structure under regular and irregular waves at various water depths, wave heights and periods in a 2D NWT. Wang and Wu [14], using a NWT based on finite element method (FEM), studied fully nonlinear interaction between waves and vertical cylinder arrays. Lal and Elangovan [15] numerically simulated waves in a 3D NWT using a flap type wave-maker. Elangovan [16] simulated and studied irregular waves in a NWT. Sriram et al. [17] used a piston type wave-maker to generate nonlinear waves in a 2D NWT. Use of a piston type wave-maker was also employed by Liang et al. [18] to generate an irregular wave train. Prasad et al. [19] in their study employed a 3D NWT to generate waves. They studied flow characteristics and reported the effect of front guide nozzle shape on primary energy conversion. Zullah et al. [20] simulated regular waves in a NWT and later on analyzed the performance of a Savonius turbine. Choi et al. [21] experimentally studied the effects of wave conditions on the performance of a cross flow turbine for wave energy conversion. Choi et al. [22] and Lee et al. [23] presented numerical and experimental results on the performance of a cross flow turbine used in a reciprocating flow for wave energy conversion.

The literature highlights the use of NWT in various fields of application ranging from naval engineering to renewable energy. The current study employs a 3D NWT based on Reynolds Averaged Navier-Stokes Equation (RANSE) to generate waves using commercial CFD code ANSYS-CFX. The free surface is captured using VOF method. After obtaining desired wave conditions, the test section is integrated into the computational domain. The test section consists of a front guide nozzle, an augmentation channel and the rear chamber. The augmentation channel houses the direct drive turbine (DDT) of cross flow type. Under the action of waves the water flows through the front guide nozzle into the augmentation channel where the turbine is located. This incoming flow rotates the turbine and flows into the rear chamber. In the rear chamber the water rises and the energy is present in form of potential energy. This potential energy then drives the turbine as the water retreats from the chamber through the turbine to the front guide nozzle. The incoming wave starts the whole cycle again. This arrangement ensures that the turbine generates power bi-directionally. Firstly, flow characteristics in the test section are studied without the turbine in the domain. This is done to understand the flow pattern under bi-directional flow. Later on the turbine is included and simulation at different rotational speeds is performed. Finally, the CFD results are validated with experimental data.

2. Methodology

2.1 Modeling

UniGraphics NX 4 CAD package was used for modeling. The length, width and height of the wave tank are 1.5 m, 1 m and 15 m respectively as shown in Fig. 1. The highlighted bold portion is the moving mesh section. The test section which consists of a front guide nozzle, front nozzle, rear nozzle, rear chamber and turbine is shown in Fig. 2. The length of the augmentation channel (front nozzle and rear nozzle) is 700 mm and the width is 700 mm. The rear chamber has a width of 700 mm as well.

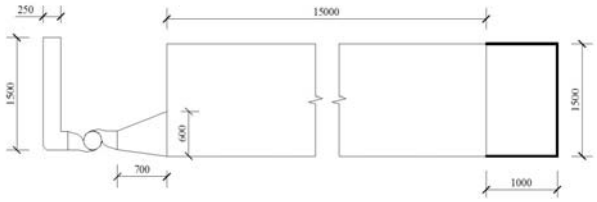

Fig. 1 Schematic of the wave tank

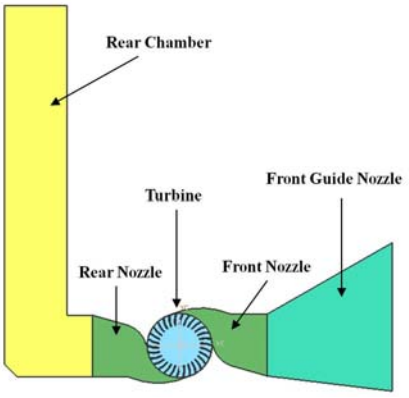

Fig. 2 Schematic of the test section

The schematic of the turbine and the runner blade is given in Fig. 3 and Table 1 shows the various parameters. The width of the turbine is 700 mm.

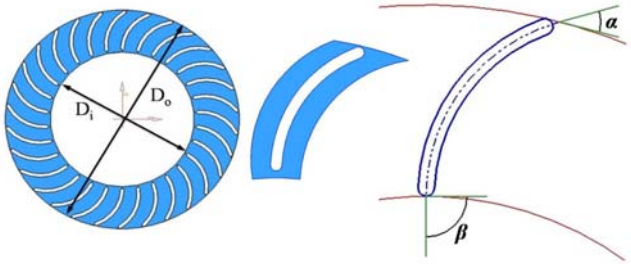

Fig. 3 Schematic of the turbine and runner blade

Table 1 Turbine and runner parameters

Parameter	Value
Blade entry angle, α	30º
Blade exit angle, β	90º
Outer Diameter, D_o	260 mm
Inner Diameter, D_i	165 mm
Number of Blades	30

2.2 Meshing

For grid generation, ICEM CFD was employed. The computational domain was discretized with hexahedral grid. The hexahedral grid or user defined meshing is used to ensure that the obtained results are of the highest quality i.e. high accuracy. The total number of nodes for all the models was 500,000. Meshing for the turbine is shown in Fig. 4. Only 1/30th model of the turbine was modeled and meshed. Once the meshing was complete, the 1/30th was copied using circular array option. This method makes for easy meshing of the complex turbine model. It is very important to capture the air water interface at the free surface accurately and for this reason the mesh near this region was refined as shown in Fig. 5.

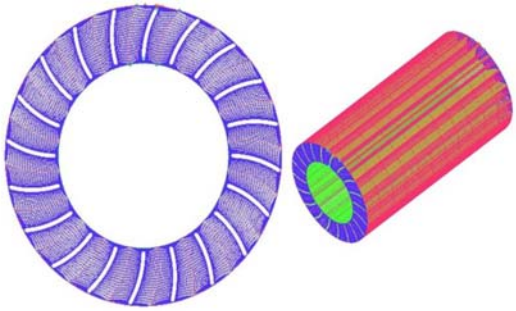

Fig. 4 Grid generation of the turbine

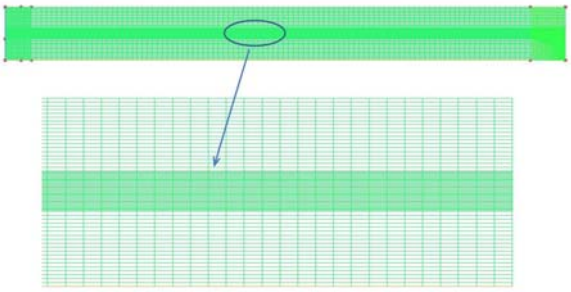

Fig. 5 Mesh refinement near the free surface

2.3 Numerical Method

Commercial CFD code ANSYS-CFX was used to simulate the waves. ANSYS-CFX is a Reynolds Averaged Navier-Stokes Equation (RANSE) solver based on Finite Volume Method (FVM) and is very helpful in multiphase simulations. The simulation type was transient and options such as homogenous multiphase, with 2nd order transient solver and coupled volume fraction were chosen. Turbulence model selected for the simulation was k-epsilon. The time discertization of the equations was achieved with the implicit second order Backward Euler scheme [24] The Volume of Fluid (VOF) method was used to capture the free surface. VOF is able to simulate the interaction between water and air at the surface very similar to that in real life. The VOF method allows tracking the amount of movement of each volume fraction of each fluid throughout the volume. [25] Using CFX Expression Language (CEL), the volume fractions of water and air were implemented. The volume fraction was set to 1 below the Mean Water Level (MWL). This represented cells filled with water. On the other hand the volume fraction above the MWL was set to 0. This represented a cell filled with air (or cell with no water) [26]. Setting these values the free surface could be captured at every time step. Any cell partially filled with air and water would represent the free surface.

The computational domain was divided into five domains; moving mesh section, NWT, front guide nozzle, augmentation channel (houses the turbine) and the rear chamber as shown in Fig. 6. The moving mesh section was employed to implement the oscillating

solid boundary of an actual wave tank. To achieve this, a wave-maker plate was incorporated. Using CEL the motion of the wave-maker plate was implemented as given by equation 1.

$$x_{dis} = A \sin \omega_0 t \quad (1)$$

where x_{dis} is displacement of the wave-maker plate in x-direction, A is the amplitude, ω_o is the frequency and t is the simulation time-step. The side walls and the bottom wall of the moving mesh section were modeled as walls with unspecified mesh motion. The top wall of the moving mesh section, NWT and the rear chamber was open to the atmosphere hence; the boundary condition was set as opening with relative pressure set to 0 Pa. The opening condition set is similar to physical wave tanks and this avoids undesirable numerical instabilities. To prevent the influence from this boundary on the formation of the surface waves the distance between the free surface and the upper boundary has to be sufficient [27]. For the current simulation the height of NWT was set to 1.5 m. The rest of the outside walls of the computational domain were modeled as solid walls where no-slip boundary condition is applied. The no-slip condition ensures that the fluid moving over the solid surface does not have a velocity relative to the surface at the point of contact. Lastly, appropriate interface regions were created. For interface, the mesh connection method was automatic.

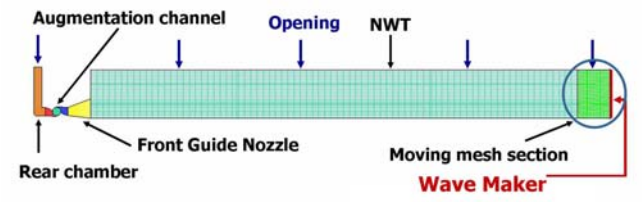

Fig. 6 Computational domain

3. Results and Discussion

3.1 Flow Characteristics

It is important to generate waves first in NWT before the rest of the model could be integrated as it saves simulation time. Formation of waves in the NWT is shown with the help of volume fraction in Fig. 7. In Fig. 7, red colour shows water and blue represents air. The air/water free surface is shown in yellowish colour. When the free surface is disturbed, waves are formed. Theses waves are sometimes called gravity waves, because it is caused by the force of gravity tending to bring the surface to its equilibrium position. Due to momentum, it overshoots the mean position and hence oscillates and the disturbance is spread to neighboring portion of the surface.

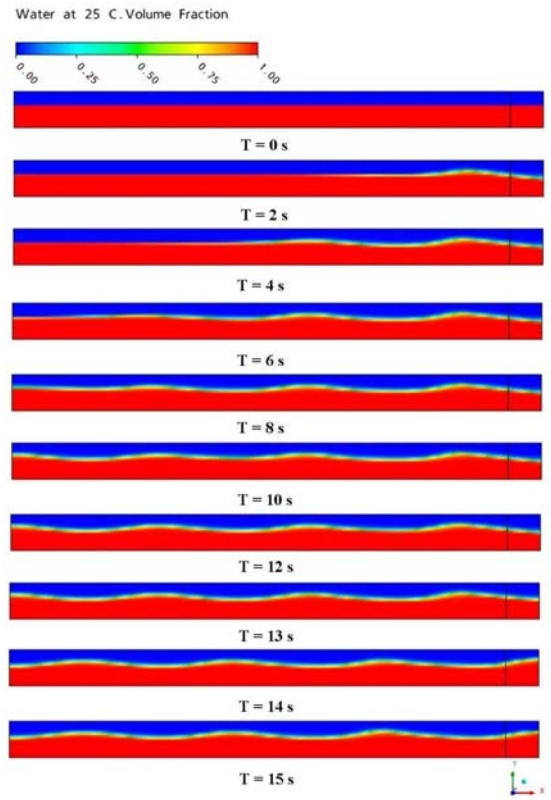

Fig. 7 Volume fraction showing formation of waves in the NWT

Figure 8 shows the wave height profile in the NWT for a time period of approximately 10 s at a point in the middle of the wave tank. The wave height and wave period was 0.2 m and 2 s respectively. Corresponding to this point the mean velocity was 0.2 m/s. The location of this point is such that it lies in line with the centre of the internal fluid region. The water velocity in the NWT is shown in Fig. 9. As expected, kinetic energy is concentrated at the surface and the velocity decreases with increasing depth. Another observation made was that the velocity slightly decreased as the waves traveled towards the rear wall of the NWT.

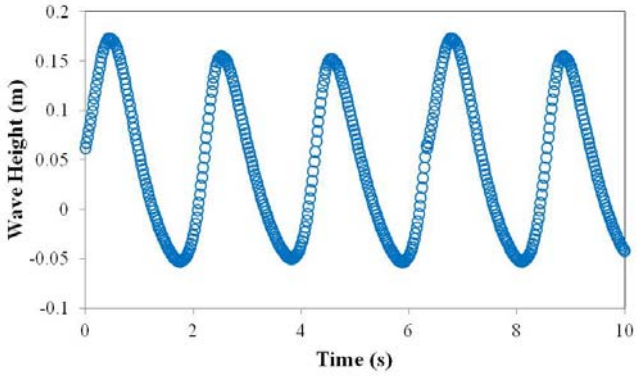

Fig. 8 Wave height in the NWT

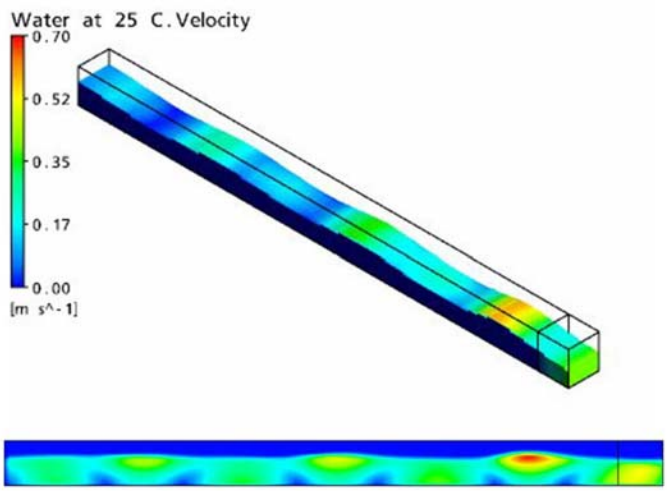

Fig. 9 Water velocity in the NWT

The velocity vector in the front guide nozzle when flow is advancing is shown in Fig. 10. There was a recirculation region observed near the top left corner, denoted by *A* when water was flowing in. Due to this, the flow was directed towards the bottom and hence higher velocity recorded in region *B*. When water was retreating, higher velocity was observed in region *A*.

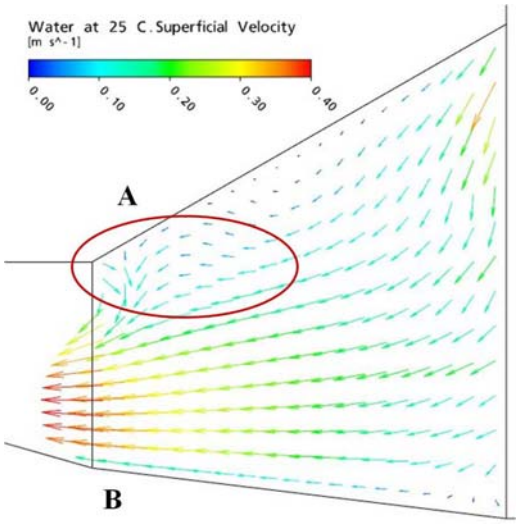

Fig. 10 Velocity vector in the front guide nozzle

Figure 11 shows velocity vectors in the augmentation channel for the advancing flow. When water is advancing, a re-circulating flow is observed in regions A and B. There is a gradual increase in the velocity in region 1. Since the rear wall is in a spiral shape, this ensures the flow enters smoothly and with uniform acceleration. On the other hand when water is flowing out of the augmentation channel vortices are observed in regions C and D.

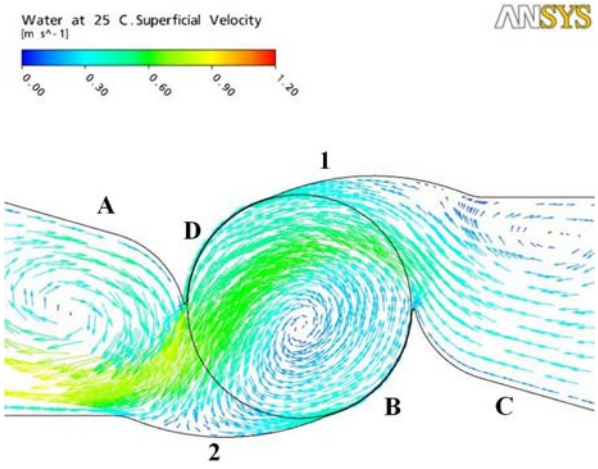

Fig. 11 Velocity vector in the augmentation channel

Power in the incoming waves was calculated using the intermediate water wave equations as given below.

$$c = \sqrt{\frac{g\lambda}{2\pi}\tanh\left(\frac{2\pi d}{\lambda}\right)} \tag{2}$$

$$c_g = \frac{1}{2}c_p\left(1+\frac{4\pi d}{\lambda}\frac{1}{\sinh\left(\frac{4\pi d}{\lambda}\right)}\right) \tag{3}$$

$$E = \frac{1}{8}\rho g H^2 \tag{4}$$

$$P_{Wave} = Ec_g \tag{5}$$

The available Water power (P_{WP}) is given by equation 7:

$$Q = \frac{V}{T} = \frac{A_{CS}\times(2\Delta Y)}{T} = \frac{2A_{CS}\Delta Y}{T} \tag{6}$$

$$P_{WP} = \rho g Q \Delta H \tag{7}$$

$$P_{Avail} = P_{Wave}\times W_G \tag{8}$$

The experimental and CFD results are shown in Table 2. The difference in the two is within 3%.

Table 2 Comparing experimental and CFD results

Variable	Unit	Experiment	CFD
H	m	0.2	0.195
T	s	2.0	2.0
ΔH	m	0.071	0.065
Q	m^3/s	0.03	0.032
P_{Wave}	W/m	86.74	82.46
P_{WP}	W/m	20.85	20.36

3.2 Turbine Performance

The turbine is now included in the computational domain and simulation at varying turbine speeds will be conducted. The speed varied from 20 to 40 rpm at intervals of 5. The turbine power, P_T and turbine efficiency, η_T were calculated using equations 9 and 10.

$$P_T = T_{ave} \times \omega \tag{9}$$

$$\eta_T = \frac{P_T}{P_{WP}} \tag{10}$$

Turbine power obtained experimentally and by CFD in the present study at different turbine speeds (rpm) is shown in Fig. 12. The turbine power increases with increasing rpm, reaches a maximum and then decreases. The peak power is obtained at 35 rpm. For CFD, the peak power is 6.71 W compared to 6.8 W obtained experimentally. The efficiency at 35 rpm is 44.73 % and 45.33 % respectively from CFD and experiments. The results obtained through CFD work are in good agreement with the experimental data. The difference is within 3%.

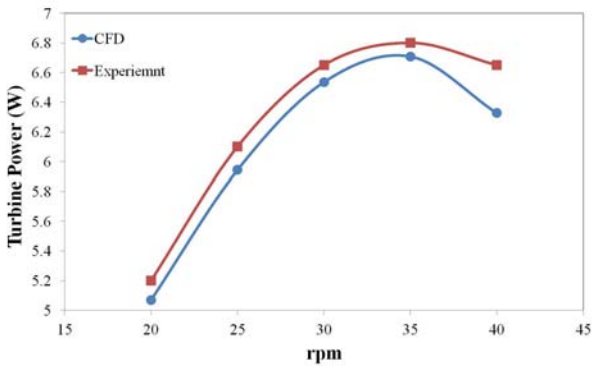

Fig. 12 Comparison between experimental data and CFD results

Average velocity recorded in the front guide nozzle at different rpm is shown in Fig. 13. The front guide nozzle inlet is denoted by $x/L_o = 0$ and the exit as $x/L_o = 1$. L_o is the length of the front guide nozzle which is 700 mm. The results show a gradual increase in velocity in the guide nozzle as desired. It is observed that the velocity increases as the rpm increases, reaches a maximum and then decreases. The trend is similar to that observed for turbine power. The highest velocity is recorded at 35 rpm while the lowest recorded at 20 rpm. This peak at 35 rpm is due to better flow characteristic as a result of which leads to better flow in the augmentation channel. This in turn results in higher turbine power as indicated in Fig 12.

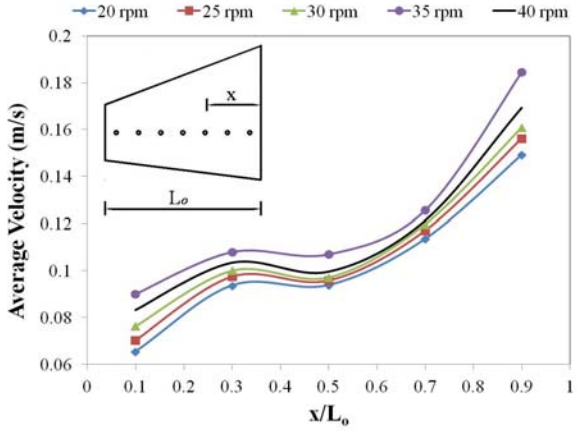

Fig. 13 Average velocity in the front guide nozzle at different rpm

Average velocity recorded at the turbine section of front nozzle exit at different rpm is shown in Fig. 14. The average was done over a 10 s period. To compare results the case with no turbine is also include in the figure. The massive difference in the velocity recorded between 0° and 50° represents power extraction form the flow. A careful look at Fig. 14 reveals that the maximum power extraction by the turbine is achieved at 35 rpm. This is why the velocity recorded is the lowest for 35 rpm compared to 20 and 40 rpm. This results in higher turbine power and higher efficiency which is highlighted in Fig. 12.

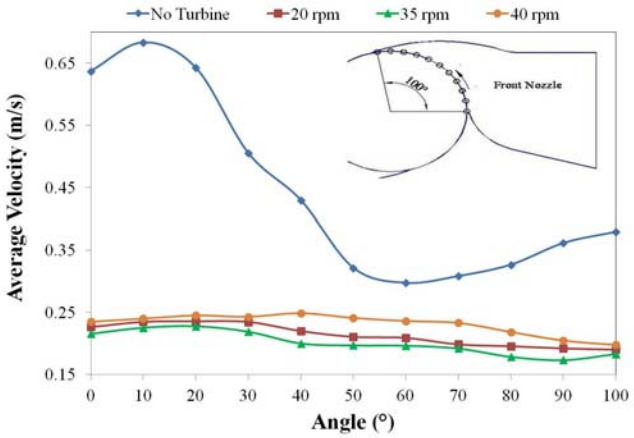

Fig. 14 Average velocity at the turbine section of front nozzle exit at different rpm

Velocity vectors in the augmentation channel when water is entering the turbine at turbine speed of 35 rpm are shown in Fig. 15. The flow accelerates approaching stage 1 as expected. The water passes through the turbine passage at stage one while imparting

energy to the runner. From the exit at stage 1 to the entry of blades at stage 2, the flow again accelerates a little. At stage 2, the passing water imparts energy to the runner once more before flowing into the rear nozzle. For advancing flow vortex is observed at bottom right portion and the position moves to top left portion when the flow retreats.

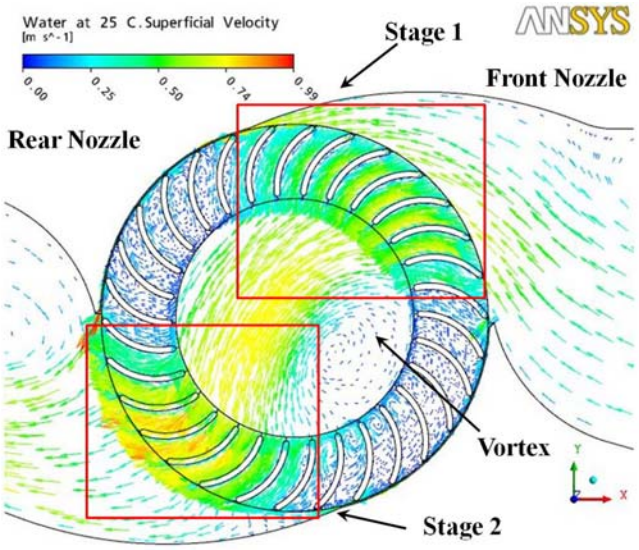

Fig. 15 Velocity vector in the augmentation channel at 35 rpm

4. Conclusions

Commercial CFD code ANSYS-CFX was successfully used to generate waves in a NWT using a piston type wave-maker. The results of CFD simulation showed good agreement with the experimental data. The difference in result was within 3%. The maximum turbine power was obtained at 35 rpm both experimentally and numerically. For CFD, the maximum power was 6.71 W compared to 6.8 W obtained experimentally. The efficiency at 35 rpm was 44.73 % and 45.33 % respectively for CFD and experiment.

REFERENCES

1. Mikkola, T., "Simulation of Plunger Type Wave Maker," J. Structural Mechanics, Vol. 40, No. 4, pp. 19-39, 2007.
2. Oliveira, T. C. A., Gironella, F. X., Sanchez Arcilla, A., Sierra, J. P. and Celigueta, M. A., "Nonlinear Regular Wave Generation in Numerical and Physical Flumes," J. Costal Research, Special Issue, No. 56, pp. 1025-1029, 2009.
3. Dean, R. G. and Dalrymple, R. A., "Water Wave Mechanics for Engineers and Scientists," World Scientific, 1991.
4. Liu, E., "Application of Numerical Wave Tank to OWC Air Chamber for Wave Energy Conversion," Proc. of the 18th Int. Offshore and Polar Eng. Conf., Vancouver, Canada, 2008.
5. Horko, M., "Optimisation of an Oscillating Water Column Energy Converter," Thesis of Master of Engineering, The University of Western Australia, 2007.
6. Repalle, N., "CFD Simulation of Wave Run-up on a Spar Cylinder," Proc. of 16th Australasian Fluid Mechanics Conf., Gold Coast, Australia, 2007.
7. Lemos, C. M., "Numerical Modeling of Shallow Water Waves: Application of the VOF Technique and k-ε Turbulence Model," PhD Thesis, Technical University of Catalonia, 1990.
8. Van Gent, M. R. A., Tones, P., Petit, H. A. H. and Van Den Bosch, P., "Wave Action on and in Permeable Structures," Proc. 24th Int. Conf. on Costal Eng., Kobe, Japan, pp. 1739-1753, 1994.
9. Dalrymple, R. A. and Rogers, B. D., "Numerical Modeling of Water Waves with SPH Method," Costal Eng., Vol. 53, No. 2-3, pp. 141-147, 2006.
10. Shao, S., Ji, C., Graham, D. I., Reeve, D. E., James, P. W. and Chadwick, A. J., "Simulation of Wave Overtopping by an Incompressible SPH Model," Costal Eng., Vol. 53, No. 9, pp. 723-735, 2006.
11. Koo, W. C. and Kim, M. H., "Numerical Simulation of Nonlinear Wave and Force generated by a Wedge-Shape Wave Maker," Ocean Eng., Vol. 33, pp. 983-1006, 2006.
12. Finnegan, W. and Goggins, J., "Numerical Simulation of Linear Water Waves and Wave-structure Interaction," Ocean Eng., Vol. 43, pp. 23-31, 2012.
13. Li, Y. and Lin, M., "Regular and Irregular Wave Impacts on Floating Body," Ocean Eng., Vol. 42, pp. 93-101, 2012.
14. Wang, C. Z. and Wu, G. X., "Interactions Between Fully Nonlinear Water Waves and Cylinder Array in a Wave Tank," Ocean Eng., Vol. 37, pp. 400-417, 2010.
15. Lal, A. and Elangovan, M., "Simulation and Validation of Flap Type Wave Maker," World Acad. Sci. Eng. Tech., Vol. 46, pp 76-82, 2008.
16. Elangovan, M., "Simulation of Irregular Waves by CFD," World Acad. Sci. Eng. Tech., Vol. 79, pp 554-558, 2011.
17. Sriram, V., Sannasiraj, S. A. and Sundar, V., "Simulation of 2-D Nonlinear Waves Using Finite Element Method with Cubic Spline Approximation," J. Fluid Struct., Vol. 22, No. 5, pp. 663-681, 2006.
18. Liang, X.-f., Yang, J.-m., Li, J., Xiao, Li.-f. and Li, X., "Numerical Simulation of Irregular Wave – Simulating Irregular Wave Train," J. Hydrodyn. Ser. B, Vol. 22, No. 4, pp. 537-545, 2010.

19. Prasad, D., Zullah, M. A., Ahmed, M. R. and Lee, Y. H., “Effect of Front Guide Nozzle Shape on the Flow Characteristics in an Augmentation Channel of a Direct Drive Turbine,” Sci. China Tech. Sci., Vol. 53, No. 1, pp. 46-51, 2010.

20. Zullah, M. A., Prasad, D., Ahmed, M. R. and Lee, Y. H., “Performance Analysis of a Wave Energy Converter Using Numerical Simulation Technique,” Sci. China Tech. Sci., Vol. 53, No. 1, pp. 13-18, 2010.

21. Choi, Y. D., Kim, C. G. and Lee, Y. H., “Effect of wave conditions on the performance and internal flow of a direct drive turbine,” J. of Mechanical Science and Technology, Vol. 23, pp. 1693-1701, 2009.

22. Choi, Y. D., Kim, C. G., Song, J. I. and Lee, Y. H., “A performance study on a direct drive hydro turbine for wave energy converter,” J. of Mechanical Science and Technology, Vol. 24. No. 11, pp. 1-10, 2010.

23. Lee, Y. H., Kim, C.G., Choi Y. D., Kim, I. S. and Hwang, Y. C., “Performance of a direct drive hydro turbine for wave power generation,” IOP Conf. Series: Earth and Environmental Science 25th IAHR Symposium on Hydraulic Machinery and Systems 2010; 12-012029.

24. Lais, S., Liang, Q., Henggeler, U., Weiss, T., Escalar, X. and Egusquiza, E., “Dynamic Analysis of Francis Runners-Experiment and Numerical Simulation,” Int. J. Fluid Machinery and Systems, Vol. 2, No. 4, pp. 303-314, 2009.

25. Gomes, M. N., Olinto, C. R., Rocha, L. A. O., Souza, J. A. and Isoldi, L. A., “Computational Modeling of a Regular Wave Tank,” Thermal Eng., Vol. 8, No. 1, pp. 44-50, 2009.

26. Maguire, A. E. and Ingram, D. M., “Wavemaking in a Commercial CFD Code,” Proc. on the 3rd Conf. on the Application of Physical Modeling to Port and Costal Protection, Barcalona, Spain, 2010.

27. Clauss, G. F., Schmittner, C. E. and Stuck, R., “Numerical Wave Tank- Simulation of Extreme Waves for the Investigation of Structural Responses,” Proc. of the OMAE 2005 24th Int. Conf. on Offshore Mechanics and Arctic Eng., Halkidiki, Greece, 2005.